Available online at www.sciencedirect.com

SciVerse ScienceDirect

Ceramics International 38 (2012) 3435–3443

CERAMICS INTERNATIONAL

www.elsevier.com/locate/ceramint

Electrophoretic deposition of nanocomposite (HAp + TiO_2) on titanium alloy for biomedical applications

L. Mohan [a], D. Durgalakshmi [b], M. Geetha [b], T.S.N. Sankara Narayanan [c], R. Asokamani [b,*]

[a] School of Biotechnology, Chemical and Biomedical Engineering, VIT University, Vellore 632014, India
[b] School of Mechanical and Building Sciences, VIT University, Vellore 632014, India
[c] NML CSIR Madras Complex Taramani, Chennai 600113, India

Received 20 August 2011; received in revised form 19 December 2011; accepted 21 December 2011
Available online 31 December 2011

Abstract

This paper reports on the corrosion and scratch behavior of TiO_2 + 50%HAp nanoceramic coated Ti–13Nb–13Zr orthopedic implant alloy. An adherent thin coating was obtained using the electrophoretic deposition (EPD) technique at 30 V and sintering at 850 °C. The microstructure of the coated surfaces was characterized by optical microscopy, AFM, and SEM, and the composition of the coating was examined using EDAX. The functional groups and formed phases analyzed using FT-IR, and XRD. Further, the adhesion strength of the coatings was evaluated using scratch tester and the corrosion behavior of all samples was tested in Simulated Body Fluid (SBF-Hank's solution) using a potentiodynamic polarization studies. The sintered coating exhibited higher adhesion, lower porosity and higher density compared to unsintered samples, and higher corrosion resistance compared to the substrate. However, the corrosion resistance of the unsintered coating was superior to that of the sintered one due to the presence of minimal interconnected porosity.

Keywords: A. Sintering; B. Nanocomposite; C. Corrosion; D. TiO_2; E. Biomedical applications; Hydroxyapatite

1. Introduction

Commercially pure Ti (CP-Ti) and Ti based alloys are extensively used for orthopedic and dental prosthetic applications [1–3] because of their superior mechanical and biocompatible properties. Currently, the alpha + beta Ti alloy *viz.*, Ti–6Al–4V is the most widely used for hip, spinal and knee replacements due to its high hardness and the CP-Ti with alpha phase for dental applications owing to its low density and high corrosion resistance. The moduli of CP–Ti (100 GPa) and Ti–6Al–4V (114 GPa) are very much higher than human bone modulus (10–30 GPa). Beta Ti alloys and near beta Ti alloys are considered to be an alternative for Ti–6Al–4V as their modulus of Elasticity (55–77 GPa) is much closer to bone when compared with the CP-Ti and Ti–6Al–4V. Among different beta alloys, the near beta alloy Ti–13Nb–12Zr is well established biomedical material for joint allocations as it exhibits low modulus and in addition, this alloy possesses highly biocompatible and non-toxic alloying elements such as Zr and Nb. However, all Ti based alloys are classified as bioinert materials as they do not induce bone formation on their surface.

It is well known that hydroxyapatite (HAp) [$Ca_3(PO_4)_3OH$] coatings have been employed since few years as they are found to increase the bioactivity of the implant surface due to the fact that they possess similar chemical, structural and biological properties to that of the human bone, which in turn promotes osseointegration [4,5]. The major advantage associated with nano HAp coatings is that the nanoparticles are similar to that of inorganic molecules of the human bone.

However, coating with HAp alone has some disadvantages such as (i) low melting point of phosphorous in the coating causing bioactive degradation of the coating [6] (ii) the HAp coated implants giving a better pinning to the bone compared with that of the adhesion between coating and the implant which will ultimately lead to loosening and failure of the implant. To overcome these problems, bioactive TiO_2 powders were added to HAp for improving bioactivity and adherence of the coating to the implant [6]. Koike et al. also have reported that TiO_2/HAp composite coatings on Ti–6Al–4V produced by

* Corresponding author. Tel.: +91 0416 2202295; fax: +91 0416 2243092.
E-mail address: geethamanivasagam@vit.ac.in (M. Geetha).

0272-8842/$36.00
doi:10.1016/j.ceramint.2011.12.056

plasma spraying technique led to increased corrosion resistance [7]. Further, Webster et al. showed that nanophase TiO_2 promotes osteoblastic adhesion compared to conventional powders [8]. The addition of nano TiO_2 to nano HAp is found to increase the adhesion of the coating with the substrate and also with the bone.

HAp/TiO_2 composite coatings on orthopedic biomaterial substrates have been obtained using several techniques such as sol–gel [9,10], micro arc oxidation [11], and plasma spraying [12]. Among these techniques, the plasma spraying technique has some drawbacks, as coatings obtained by this method can be easily detached from the surfaces or resorbed into the body environment because of their unstable characteristics such as rapid solidification, inhomogeneous composition, melted and decomposed phases, *etc.*, [13].

Electrophoretic Deposition (EPD) has been found to be an efficient technique to make ceramic coatings from powder suspensions and it is an easier process for obtaining nanostructural deposits from colloidal solutions. The other advantages of EPD technique are that it is less time consuming, less expensive and it leads to uniform coatings and that can be obtained on any complex shapes too [14,15]. Nathanael et al. who worked on nanocomposite coatings with 50 as well as 80 vol% of TiO_2 added to HAp reported better mechanical properties compared to HAp. It should be noted that these coatings were produced on plain glass substrates [10], whereas in this work a 1:1 HAp/TiO_2 nanocomposite coating on the low-modulus FDA-approved Ti–13Nb–13Zr (ASTM F 1713–08) biomedical alloy was produced, hence these studies should be more relevant.

2. Materials and methods

2.1. Preparation of nano-HAp

Hydroxyapatite nanoparticles were prepared by a wet chemical technique in which the starting materials are $CaCl_2{\cdot}2H_2O$, $(NH_4)_2HPO_4$ and NH_4OH (Aldrich). HAp precipitate was prepared by slow addition of 0.6 M ammonium phosphate solution to a 1.0 M calcium chloride dehydrate solution at 70 °C. The pH was monitored and adjusted to 11 by addition of NH_4OH to the medium. The mixture was thoroughly stirred for 8 hrs while maintaining the temperature at 70 °C, and then dried at room temperature for one day. Finally, the precipitate was washed with water and isopropyl alcohol [16]. HAp obtained was characterized using XRD for phase confirmation and size determination.

2.2. Preparation of nano-TiO_2

TiO_2 nanoparticles were prepared using $TiCl_4$, distilled water and NH_4OH (Aldrich). $TiCl_4$ was added to distilled water at 2–3 °C and maintained in same conditions for 12 hours. NH_4OH solution was added to the above solution and stirred well until $Ti(OH)_2$ and ammonium chloride got precipitated. The pH of the above reaction was kept constant at 8. The obtained precipitate was filtered twice, first using normal distilled water and then using hot distilled water to remove chloride ions present in the precipitate. It was dried using a furnace maintained at 200 °C for 24 hrs. Heating removed hydroxyl (OH^-) ions leaving behind TiO_2. The TiO_2 precipitates were characterized using XRD to determine the phases, size and compounds present.

2.3. Sample preparation

Test samples, 10 mm × 10 mm × 50 mm of titanium alloy Ti–13Nb–13Zr cut from sheets were ground with 200 to 1200# grit silicon carbide paper and polished using 0.5 μ alumina powder. These samples were ultrasonically cleaned using acetone and then pickled in 25% of HNO_3 for 10 min in order to remove oxide layers over the substrate.

2.4. Suspension preparation for electrophoretic deposition

Several solvents such as acetone, n-butanol, and carbon tetra chloride with additives such as PVP (poly vinyl pyrrolidone), PEG (poly ethylene glycol), PEI (poly ethylene amine), and iodine were used for preparing the suspension. The sample Ti-13-13 acted as cathode and 316SS acted as anode. Both were immersed in a suspension containing beaker. The voltage was set at 30 V and the deposition time was 5 min. In the preparation of suspension, 0.25 g of nano composite powders (HAp + TiO_2) was added to 15 ml of solvent and sonicated for 10 min. Following this, iodine (0.1 g) was added as it acts as a dispersant to stabilize the suspension. The precursor (dispersant/binder used to stabilize the suspension) used for the preparation of suspension was determined by repeated trials. The uniform coatings obtained using the suspension prepared out of iodine and acetone were subjected to detailed characterization.

2.5. Sintering of coated samples

In order to increase the adhesion strength of the coating and decrease the porosity, the coated samples were sintered. Generally, high temperature is required for the complete densification of the coating and the sintering temperatures are chosen in such a way it does not alter the bulk specimen properties. It is well known that during sintering the coatings may fail due to mismatch between thermal expansion coefficients. The thermal expansion coefficient of Ti substrate ($\alpha Ti = 8.7 \times 10^{-6}/K$), is much lower than that of HAp ($\alpha HAp = 13.6 \times 10^{-6}/K$), and this large thermal expansion mismatch leads to the formation of cracks in coatings when cooled from elevated temperature [17]. The addition of TiO_2 to HAp, with relatively lower thermal expansion coefficient ($\alpha TiO_2 = 7.249 \times 10^{-6}$), will lead to a thermal expansion mismatch reduction between HAp and Ti alloy.

To achieve denser coatings, the sintering process was carried out at the heating rate of 10 °C/min in the furnace and maintained at 850 °C for 2 hrs with 20 ml/min flow of argon gas. Cooling rate was maintained at 10 °C/min to room temperature.

2.6. Characterization techniques

The phases formed in the nanocomposite coating were investigated by X-ray diffraction (XRD) using PHILIPS X-ray diffractometer (BRUKER, Germany). A monochromatic source, Cu Kα radiation (λ = 0.1548 nm) was used and the samples were scanned from 0° to 80° at a scanning rate of 0.5°/min. The Fourier Transform Infrared (FT-IR) spectrum was recorded to determine the functional group in synthesized HAp and TiO_2 powders and composite coatings using 330 FT-IR AVATAR THERMO NICOLET. For this, 2 mg of coatings scraped from the sample was mixed with 200 mg spectroscopic grade potassium bromide (KBr) and the spectra were collected in the wave number range 4000–400 cm^{-1}. The microstructures of the deposited composite coatings were studied using optical microscope (OM, ZEWASS-CLEMEX VWASION), atomic force microscopy (Easy Scan 2, Nanosurf, Switzerland), scanning electron microscopy (SEM, HITACH 3500N). For elemental analysis, energy dispersive X-ray spectroscopy (EDAX, HITACH 3500N) was carried out in addition to SEM. The porosity of the coated samples was analyzed from SEM images using Materials Pro 3.0 software.

The adhesion strength of the coating to the substrate was evaluated using a scratch tester (DUCOM) with a Rockwell C diamond indenter having tip radius of 200 microns. The instrument was operated using WINDUCOM software installed in the computer attached to the scratch tester. The ramp load was varied from 1 N to 7 N for analyzing adhesion strength and the stroke length was kept as 5 mm with scratch speed of 1.00 mm/sec in ramp. After the scratch testing, the morphology of the scratched area was observed using an optical microscope.

Potentiodynamic polarization studies were performed using a POTENTIOSTAT (ACM Gill AC, version 5), interfaced with a computer. The investigated potential range was adjusted to be from −500 mV (SCE) to 2500 mV (SCE) with a scan rate of 10 mV/min. A conventional three-electrode cell arrangement was used for the corrosion measurement, with a Saturated Calomel Electrode (SCE) as a reference electrode and platinum foil as the counter electrode. The naturally aerated Hanks' solution was used to simulate the physiological medium for the pH of 7.4 and the experiments were carried out at room temperature. The composition of Hank's solution which is very similar to our human physiological fluids, was prepared up to 1 liter with 0.185 g $CaCl_2$ (1.258 mol), 0.4 g KCl (0.00536 mol), 0.06 g KH_2PO4 (0.0004 mol), 0.1 g $MgCl_2{\cdot}6H_2O$ (0.00049 mol), 0.1 g $MgSO_4{\cdot}7H_2O$ (0.00041 mol), 8.0 g NaCl (0.137 mol), 0.35 g $NaHCO_3$ (0.00417 mol), 0.48 g Na_2HPO_4 (0.00269 mol) and 1.00 g D $C_6H_{13}NO_5HCl$ (0.004637 mol)

3. Results and discussion

3.1. XRD analysis

The phases formed in the synthesized nano HAp and nano TiO_2 powders were investigated using XRD analysis and illustrated in Fig. 1. The XRD pattern of the synthesized nano HAp powder was compared with JCPDS#9-432, which

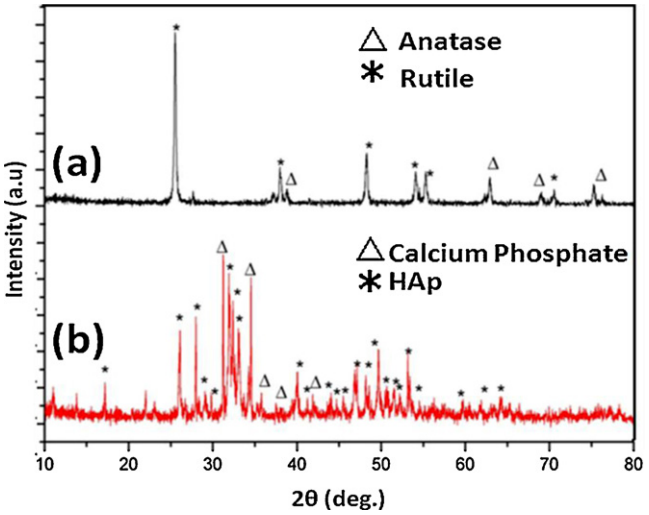

Fig. 1. X-ray diffraction pattern for synthesized nano TiO_2 (a) and HAp powder (b).

confirmed the presence of the hydroxyapatite along with some amount of calcium phosphate (JCPDS#21-839). The presence of calcium phosphate in the coating mimics the bone composition and gives an added advantage because it leads to enhanced osseointegration. Similarly the XRD pattern of the prepared nano TiO_2 was compared with JCPDS#88-1175 for rutile TiO_2 and JCPDS#84-1286 for anatase TiO_2 phases. Fig. 2 reveals the presence of a larger number of peaks corresponding to the anatase phase compared to the rutile phase. The sharp peaks of TiO_2 suggest that its structure is polycrystalline. The sizes of the prepared nano HAp and nano TiO_2 powders were calculated using Scherer's formula ($d = 0.9\lambda/\beta \cos\theta$, where λ – wavelength of X-rays, β – FWHM of diffraction peak, θ – angle corresponding to the peak) were 35 nm and 65 nm respectively. The XRD analysis of sintered and unsintered coatings also confirms the presence of HAp, Calcium phosphate and anatase

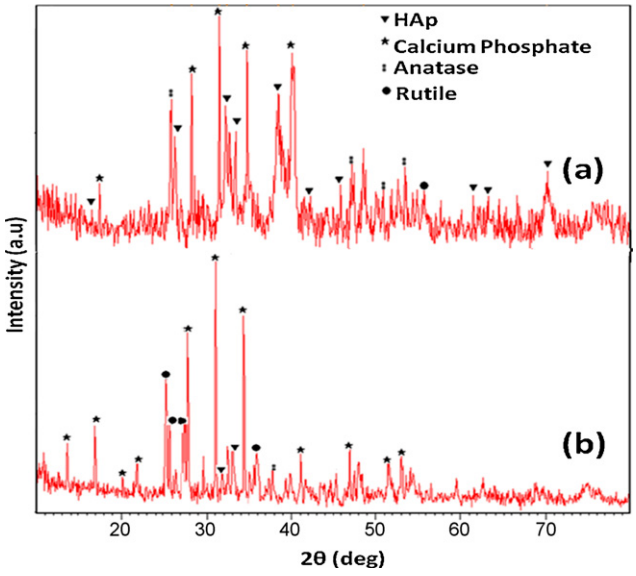

Fig. 2. X-ray diffraction pattern for nano Hap/TiO_2 coated samples (a) before sintering and (b) after sintering.

and rutile phase of TiO_2. Maximum intensity corresponding to the HAp + calcium phosphate in the sintered sample was observed in XRD analysis, when compared with that of the unsintered. Sharp peaks corresponding to the composites are also observed after sintering, which supports the formation of crystalline HAp and calcium phosphate composite on sintering. On the other hand, the XRD analysis of TiO_2 coated surface revealed the formation of the rutile phase of TiO_2 indicating that the anatase phase of TiO_2 is converted into the rutile phase on sintering.

3.2. FT-IR analysis

The infrared spectra of nano HAp (Fig. 3) shows absorption in three regions: (i) the band at 3751^{-1} cm^{-1} and the libration band at 632^{-1} cm^{-1} are originated from OH^- group. (ii) The bands at 963 cm^{-1} are characteristic bands of PO_4^{3-} ions (υ_1 band), 1090 and 1052 cm^{-1} (υ_3 band) and 566 and 602 cm^{-1} (υ_4 band). (iii) The presence of 1634 cm^{-1} peak confirms the presence of carbonate group [18,19]. FT-IR analysis of nano TiO_2 (Fig. 4) gives a clear picture of a broad band area with small absorption peaks of bulk titania with anatase (632–520 cm^{-1}) and rutile (449 cm^{-1}) phases from 400 to 800 cm^{-1} [20]. The FT-IR of composite coating consisting of HAp/TiO_2 (Fig. 5) clearly illustrates the presence of both phases of Titania (400–800 cm^{-1}) and also the presence of all the three regions corresponding to HAp.

3.3. Surface morphology

3.3.1. Optical microscopy

Fig. 6a and b shows the optical microscopy images of a composite HAp/TiO_2 coating of Ti–13Nb–13Zr before and after sintering at 850 °C respectively. After sintering, the coating was observed to be denser when compared to the unsintered sample. It is clearly evident from Fig. 6b that the pores present in the coating are also completely filled after sintering. Hence sintering has to be carried out for a uniform

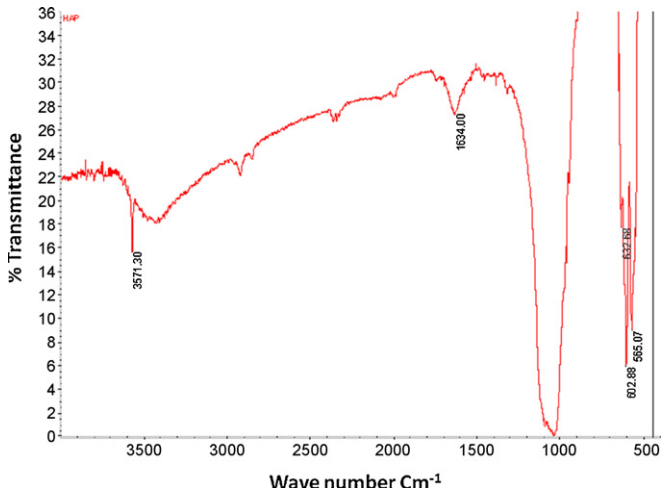

Fig. 3. FT-IR spectrum of as-prepared nano HAp powder.

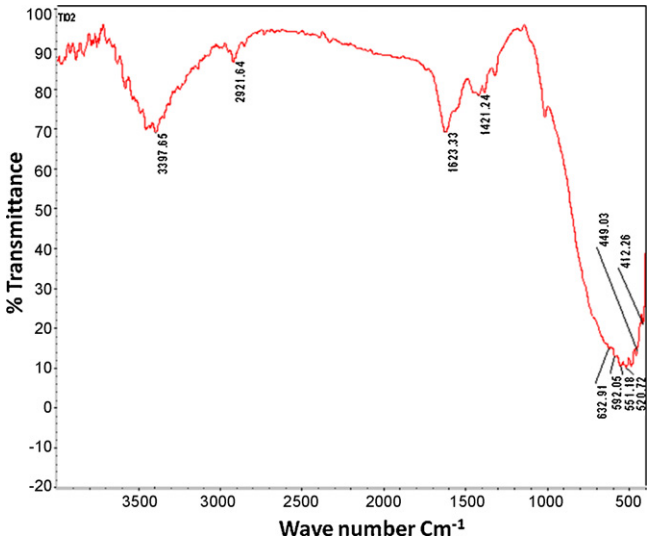

Fig. 4. FT-IR spectrum of as-prepared nano TiO_2 powder.

coating formation of nanocomposite HAp/TiO_2. This observation is further corroborated by AFM and SEM analysis and discussed in detail in Sections 3.3.2 and 3.3.3.

3.3.2. Atomic force microscopy

The surface roughness and the thickness of the coated surface were analyzed using AFM 3-D surface imaging using AFM. Fig. 7b shows that the coating after sintering was dense with less porosity compared with the unsintered coating (Fig. 7a). We observe that the roughness of sintered coating (0.38 μm) was reduced by 0.05 μm compared to the unsintered coating (0.43 μm). Sintering has an effect on thickness also, as expected, and the thickness of the sintered coating was found to be 3.71 μm which was reduced by 0.04 μm compared with that of unsintered coating (4.01 μm).

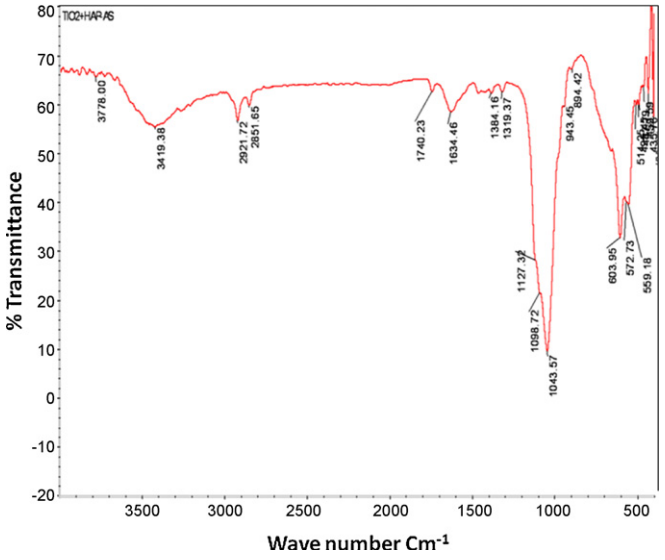

Fig. 5. FT-IR spectrum of nanocomposite HAp/TiO_2 coating after sintering.

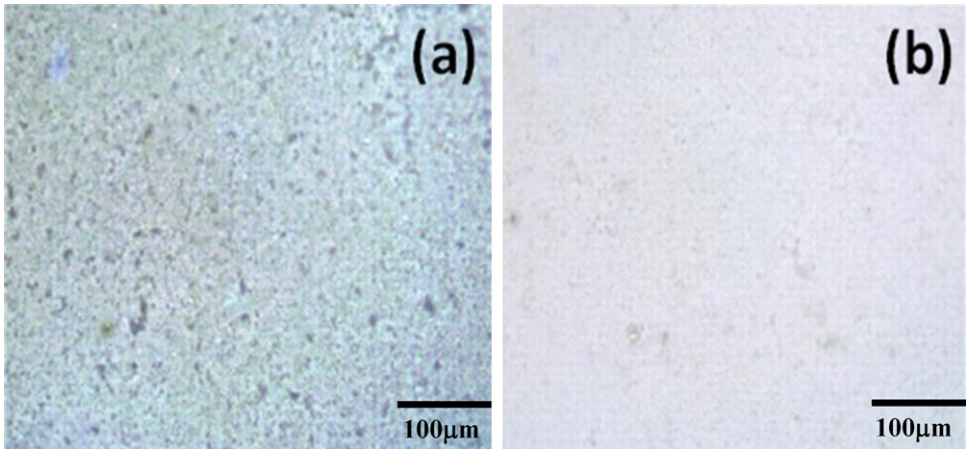

Fig. 6. Optical images of HAp/TiO_2 coated samples (a) before sintering and (b) after sintering.

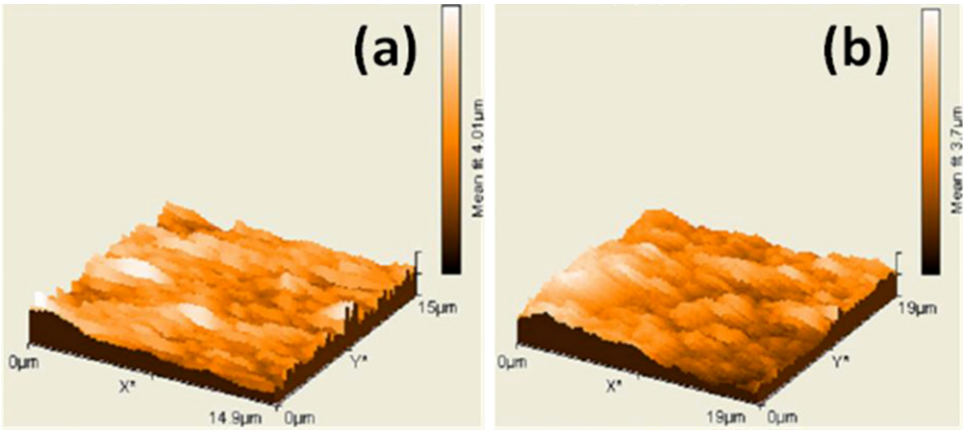

Fig. 7. AFM 3D images of HAp/TiO_2 coated samples show the surface thickness (a) before sintering and (b) after sintering.

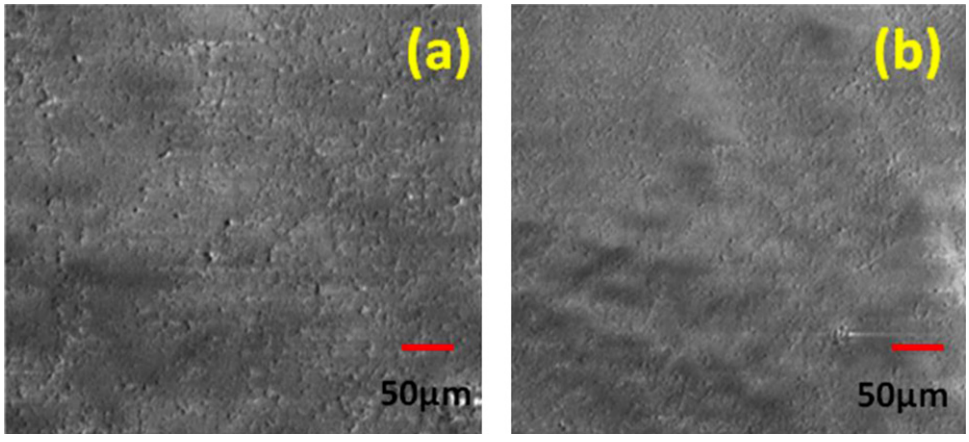

Fig. 8. SEM images of HAp/TiO_2 coated samples (a) before sintering and (b) after sintering.

3.3.3. Scanning electron microscopy with EDAX

SEM images of sintered and unsintered coatings are shown in Fig. 8a and b. SEM micrographs reveal the formation of a uniform coating with no cracks in both the sintered and unsintered conditions. Under high magnification, it has been observed that after sintering there is grain growth and enhanced bonding between the composite particles (Fig. 9a and b). Grain growth is associated with volume expansion due to oxidation reaction of $Ti \rightarrow TiO_2$, which partially compensates for the sintering shrinkage and thus prevents crack formation. On the other hand, the unsintered coating exhibits large number of free standing and partially bonded composite particles.

The porosity of the coated samples was measured using SEM images with material PRO software for sintered (Fig. 10a) and unsintered (Fig. 10b) coatings. It was observed that the total porosity count of the sintered sample was less (96 counts) when

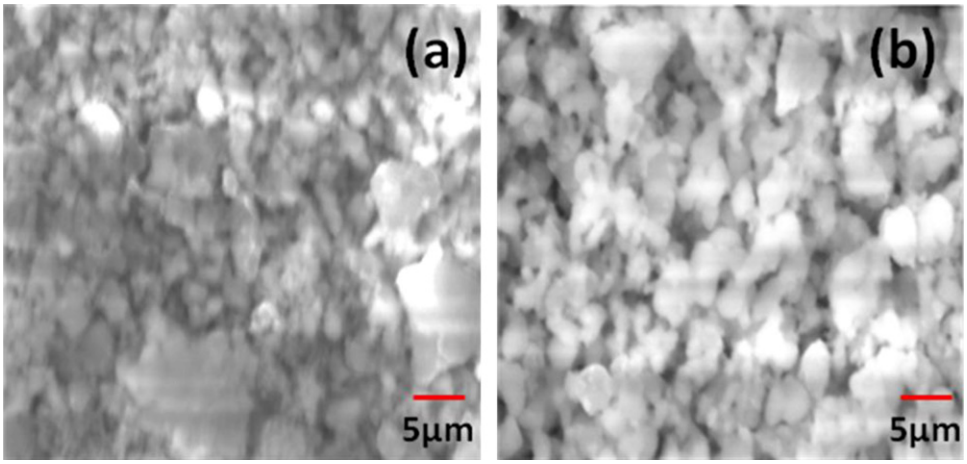

Fig. 9. SEM images of HAp/TiO_2 coated samples (a) Before sintering and (b) After sintering.

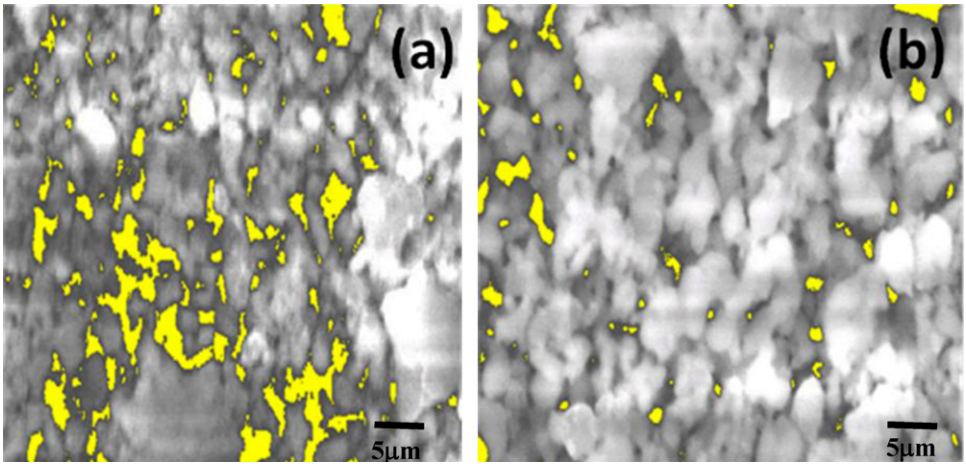

Fig. 10. Porosity of HAp/TiO_2 coated samples (a) before sintering and (b) after sintering.

compared to the unsintered sample (186 counts). It should be noted that the presence of porosity is advantageous as it enhances the osseointegration [21].

The elemental composition of the coating surface was examined by SEM-EDAX (Fig. 11). The analysis revealed the presence of Ca, P, O of HAp Ti, O of TiO_2 compounds

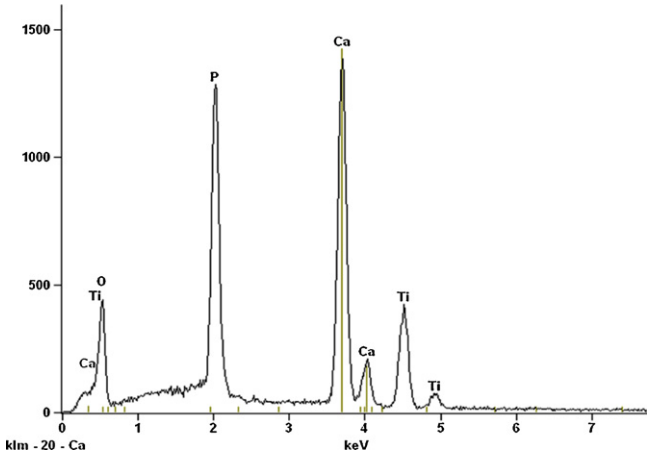

Fig. 11. EDAX for HAp/TiO_2 coated samples after sintering.

respectively. The quantitative measurements of all the elemental compositions of the coating (Table 1) were approximately equal to the stoichiometric ratio of HAp and TiO_2 and this confirmed the stability of the suspension.

3.4. Adhesion analysis using scratch tester

Both the sintered and unsintered (Fig. 12a and b) samples were subjected to scratch testing and the scratched samples were analyzed using OM. The micrograph of unsintered sample shows the substrate in the scratched area, indicating that coating has undergone gross spallation. On the other hand, in the case of sintered sample a thin layer of coating was observed after scratching. However, chipping of coating and smearing of the coated particles were also observed. These results well corroborate the studies made by Moskalewicz et al., on TiO_2 coated Ti–6Al–7Nb alloy [21]. The smearing of the particles on this surface is attributed to the softness of the coating. The presence of a thin layer of coating on the scratched surface of the sintered alloy clearly indicates that the adherence of the coating is superior when compared to the unsintered sample. The traction force of the coating was also measured from scratch analysis, and the traction forces of sintered and

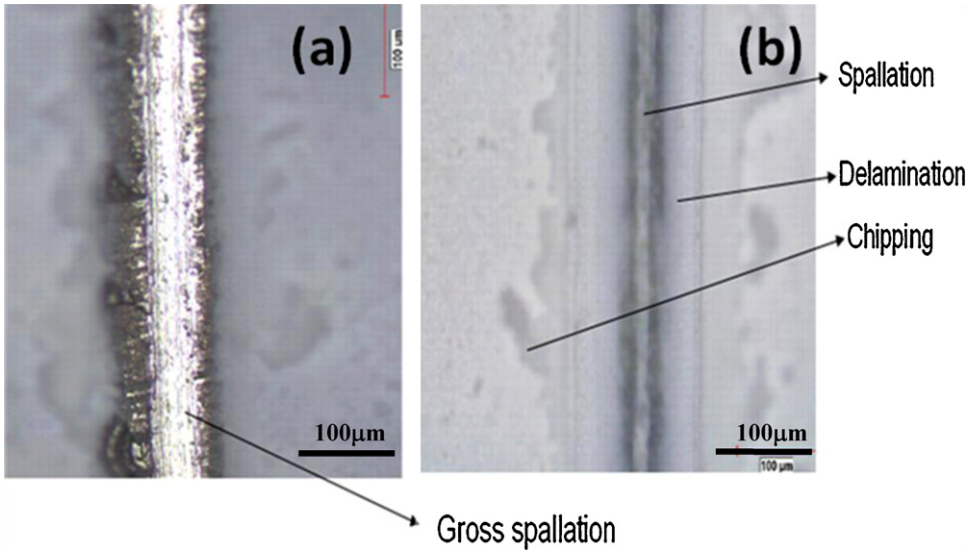

Fig. 12. Adhesion analysis using scratch tester for HAp/TiO_2 coated samples (a) before sintering and (b) after sintering.

unsintered coatings are 1.34 N and 1.54 N. The lower traction force of the sintered coating when compared to unsintered coating indicates the better adherence of sintered coating over the Ti–13Nb–13Zr substrate. When the scratch test was performed under ramp loading condition it was observed (Fig. 13) that as loading increases, the traction force raises up to a certain loading value and then remains constant for the sintered coatings. On the contrary, there was a continuous increase in traction force with loading for the unsintered coating. These results indicate that unsintered coatings adhere weakly to the substrate and hence are unable to withstand higher loads, whereas the sintered coatings offer higher resistance to scratch even at higher loads.

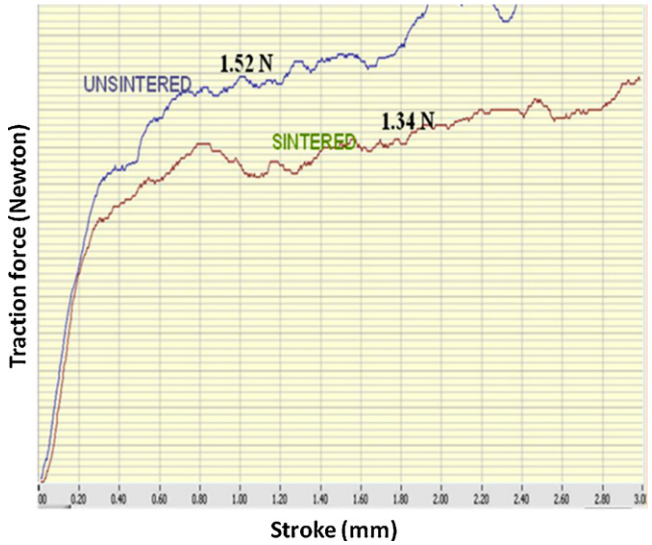

Fig. 13. Traction force analysisof HAp/TiO_2 coated samples before and after sintering.

3.5. Corrosion analysis

The potentiodynamic polarization curves of the uncoated Ti–13Nb–13Zr and HAp/TiO_2 composite coated Ti–13Nb–13Zr in freshly prepared simulated body fluid (SBF) Hank's solution are shown in Fig. 14. The corrosion current (I_{Corr}) was obtained from the polarization curves by extrapolation of the anodic and cathodic branches of the polarization curves to the

Table 1
EDAX analysis of the HAp/TiO_2 coated sample after sintering.

Element	wt%	at.%
O	33.38	54.89
P	16.28	13.83
Ca	33.91	22.26
Ti	16.42	9.02
Total	100.00	100.00

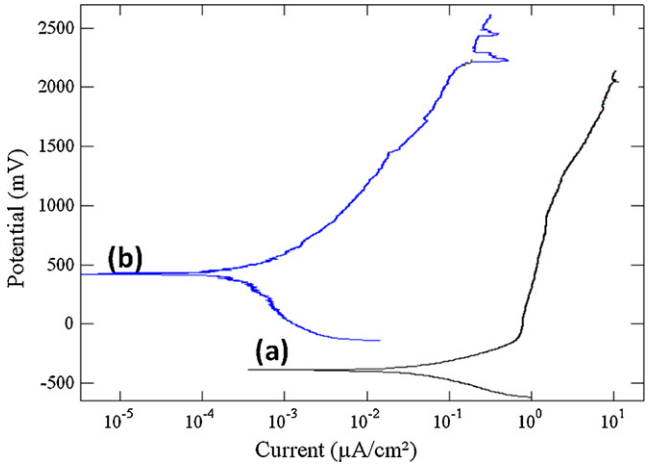

Fig. 14. Potentiodynamic polarization curves for (a) bare substrate (Ti–13Nb–13Zr) and (b) HAp/TiO_2 coated Ti–13Nb–13Zr sample.

Table 2
Potentiodynamic polarization results for bare substrate (Ti–13Nb–13Zr) and HAp/TiO_2 coated Ti–13Nb–13Zr sample.

S. No.	Sample	E_{Corr} (mV)	I_{Corr} (mA/cm^2)	Polarization resistance (Ohm cm^2)	Corrosion rate (Mills/year)
1.	Ti–13Nb–13Zr substrate	−363.96	3.442E−5	2.99E5	0.02692
2.	HAp/TiO_2 coated sample	358.79	1.864E−6	5.52E6	0.00145

corrosion potential. Table 2 shows the corrosion current density, corrosion potential and corrosion rate (mpy) for the same. The corrosion current density (I_{corr} = 3.442E−5 mA) was measured for the uncoated Ti–13Nb–13Zr (Fig. 14a and Table 2) was found to be higher when compared with the HAp/TiO_2 composite coated Ti–13Nb–13Zr (I_{corr} = 1.864E−6 mA) (Fig. 14b and Table 2). Thus the HAp/TiO_2 composite coating resulted in an increase in the corrosion resistance of the metallic substrate. A similar kind of observation has been made by Fathi et al. for HAp coatings [22] and Nikita Zaveri et al. for TiO_2 coatings on implant materials in simulated body fluids [23]. The E_{corr} value for coated sample (358.79 mV) shifted to much nobler value compared to substrate (−363.96 mV) and this result further confirms that the coated samples have superior passivation when compared to the substrate. This is further substantiated as there was a decrease in the polarization resistance and an increase in the corrosion rate of the substrate (2.99E5 (Ω) and 0.02692 mpy) and an increase in the polarization resistance and a decrease in the corrosion rate of coated sample (5.52E6 (Ω) and 0.00145 mpy), respectively. These results confirm that the coated layer possess better corrosion resistance than the native oxide layer of the substrate.

4. Conclusions

Since individual nano HAp and nano TiO_2 coatings have already proved to be biocompatible and provide higher osseointegration, an effort has been made to produce nanoceramic HAp and TiO_2 composite coatings by EPD on Ti–13Nb–13Zr alloy. The coated samples were characterized by various techniques and tested for their corrosion resistance. The following conclusions were drawn from the above experimental evidence.

i. The XRD and FT-IR analyses confirm the presence of both HAp and TiO_2 compounds in the coatings and the sizes of the synthesized particles determined from the XRD pattern are 35 nm and 62 nm respectively
ii. The microstructures of the unsintered and sintered samples examined using optical microscopy and SEM–EDAX confirmed that the coated surface of the sample sintered at 850 °C was densely packed with less porosity. The factors which are responsible for this are grain growth, bonding with the adjacent molecules and volume expansion of the coated particles.
iii. The surface morphology investigated using AFM reveals that surface roughness of the sintered coating decreased from 0.43 μm to 0.38 μm, whereas its thickness was reduced from 4.01 μm to 3.7 μm.
iv. The strength and adhesion of the sintered coating measured using scratch tester was increased by 1.14 times than the unsintered coating.
v. The HAp/TiO_2 coated sample exhibited nobler passive potential and lower corrosion current and corrosion rate when compared to the uncoated Ti–13Nb–13Zr sample.

In addition to the above, as the adhesion strength of the sintered coating is higher that of the unsintered sample, the sintered sample can be recommended for further *in vitro* testing to be considered for the final applications.

Acknowledgment

The authors would like to thank CSIR, New Delhi for funding the project.

References

[1] F.J. Gil, A. Padrós, J.M. Manero, C. Aparicio, M. Nilsson, J.A. Planell, Growth of bioactive surfaces on titanium and its alloys for orthopaedic and dental implants, Mater. Sci. Eng. C. 22 (2002) 53–60.
[2] M. Geetha, A.K. Singh, R. Asokamani, A.K. Gogia, Ti based biomaterials, the ultimate choice for orthopaedic implants – a review, Progr. Mater. Sci. 54 (2009) 397–425.
[3] S.A. Brown, J.E. Lemons, Medical applications of titanium and its alloys: the material and biological issues, ASTM STO 1272 (1996) 117.
[4] X. Pang, I. Zhitomirsky, Electrophoretic deposition of composite hydroxyapatite–chitosan coatings, Mater. Charact. 58 (2007) 339–348.
[5] M. Manson, C.J. Nez, C. Morant, P. Herrero, J.M.M.H. Nez-Duart, Electrodeposition of hydroxyapatite coatings in basic conditions, Biomaterials 21 (2000) 1755–1761.
[6] C.S. Chien, C.L. Chiao, T.F. Hong, T.J. Han, T.Y. Kuo, C.T. Lim, Synthesis and characterization of TiO_2 + HA coatings on Ti–6Al–4V substrates by Nd-YAG laser cladding, in: J.C.H. Goh (Ed.), ICBME 2008 Proceedings, vol. 23, 2009, pp. 1401–1404.
[7] M. Koike, H. Fujii, The corrosion resistance of pure titanium in organic acids, Biomaterials 22 (2001) 2931–2936.
[8] T.J. Webster, R.W. Siegel, R. Bizios, Osteoblast adhesion on nanophase ceramics, Biomaterials 20 (1999) 1221–1227.
[9] E. Milella, F. Cosentino, A. Licciulli, C. Massaro, Preparation and characterisation of titania/hydroxyapatite composite coatings obtained by sol–gel process, Biomaterials 22 (2001) 1425–1431.
[10] A. Joseph Nathanael, D. Mangalaraj, N. Ponpandian, Controlled growth and investigations on the morphology and mechanical properties of hydroxyapatite/titania nanocomposite thin films, Compos. Sci. Technol. 70 (2010) 1645–1651.
[11] Z. Yong, H. Ping, X. Kewei, H. Yong, Influence of Ca concentration in electrolyte and hydrothermal conditions on the morphology and composition of the TiO_2/hydroxyapatite composite layer by microarc oxidation, Rare Metal Mater. Eng. (2003) 12.
[12] V. Cannillo, L. Lusvarghi, A. Sola, Production and characterization of plasma-sprayed TiO_2–hydroxyapatite functionally graded coatings, J. Eur. Ceram. Soc. 28 (2008) 2161–2169.

[13] C.E. Wen, W. Xu, W.Y. Hu, P.D. Hodgson, Hydroxyapatite/titania sol–gel coatings on titanium–zirconium alloy for biomedical applications, Acta Biomater. 3 (2007) 403–410.
[14] Y. Fukada, N. Nagarajan, W. Mekky, et al., Deposition – mechanisms, myths and materials, J. Mater. Sci. 39 (2004) 787–791.
[15] L. Besra, M. Liu, Progr. Mater. Sci. 52 (2007) 1–61.
[16] I. Zhitomirsky, L. Gal-Or, Electrophoretic deposition of hydroxyapatite, J. Mater. Sci. Mater. Med. 8 (1997) 213–219.
[17] Z.-C. Wang, Y.-J. Ni, J.-C. Huang, Fabrication and characterization of HAp/Al_2O_3 composite coating on titanium substrate, Biomed. Sci. Eng. 1 (2008) 190–194.
[18] S. Raynaud, E. Champion, D. Bernache-Assollant, P. Thomas, Calcium phosphate apatites with variable Ca/P atomic ratio. I: Synthesis, characterisation and thermal stability of powders, Biomaterials 23 (2002) 1065–1072.
[19] A. Rapacz-Kmita, A.Ś. lósarczyk, Z. Paszkiewicz, C. Paluszkiewicz, Phase stability of hydroxyapatite–zirconia (HAp–ZrO_2) composites for bone replacement, J. Mol. Struct. 704 (2004) 333–340.
[20] H. Jensen, A. Soloviev, Z. Li, E.G. Søgaard, XPS and FTIR investigation of the surface properties of different prepared titania nano-powders, Appl. Surf. Sci. 246 (2005) 239–249.
[21] T. Moskalewicz, A. Czyrska-Filemonowicz, A.R. Boccaccini, Microstructure of nanocrystalline TiO_2 films produced by electrophoreticdeposition on Ti–6Al–7Nb alloy, Surf. Coating Technol. 201 (2007) 7467–7471.
[22] M.H. Fathi, F. Azam, Novel hydroxyapatite/tantalum surface coating for metallic dental implant, Mater. Lett. 61 (2007) 1238–1241.
[23] N. Zaveri, G.D. McEwen, R. Karpagavalli, A. Zhou, Biocorrosion studies of TiO_2 nanoparticle-coated Ti–6Al–4V implant in simulated biofluid, J. Nanopart. Res. (2011), doi:10.1007/s11051-009-9699-6.